

Extraction of electric field in heavily irradiated silicon pixel sensors

A. Dorokhov^{ab*}, Y. Allkofer^a, C. Amsler^a, D. Bortoletto^c, V. Chiochia^a, L. Cremaldi^d, S. Cucciarelli^e, C. Hörmann^{ab}, D. Kim^f, M. Konecki^e, D. Kotlinski^b, K. Prokofiev^{ab}, C. Regenfus^a, T. Rohe^b, D. Sanders^d, S. Son^c, T. Speer^a, M. Swartz^f

^aPhysik Institut der Universität Zürich-Irchel, 8057 Zürich, Switzerland

^bPaul Scherrer Institut, 5232 Villigen, Switzerland

^cPurdue University, Task G, West Lafayette, IN 47907, USA

^dMississippi State Univ., Department of Physics and Astronomy, MS 39762, USA

^eInstitut für Physik der Universität Basel, 4056 Basel, Switzerland

^fJohns Hopkins University, Baltimore, MD 21218, USA

A new method for the extraction of the electric field in the bulk of heavily irradiated silicon pixel sensors is presented. It is based on the measurement of the Lorentz deflection and mobility of electrons as a function of depth. The measurements were made at the CERN H2 beam line, with the beam at a shallow angle with respect to the pixel sensor surface. The extracted electric field is used to simulate the charge collection and the Lorentz deflection in the pixel sensor. The simulated charge collection and the Lorentz deflection is in good agreement with the measurements both for non-irradiated and irradiated up to 10^{15} $n_{\text{eq}}/\text{cm}^2$ sensors.

PACS: 29.40.Gx; 29.40.Wk; 61.80.-x

Key words: Electric field; Radiation hardness; Lorentz angle; Charge collection; Silicon; Pixel; CMS;

1. Introduction

The properties of the silicon sensors designed for the CMS pixel detector [1] will change during the LHC operation. The innermost barrel layer of the CMS pixel detector is expected to be exposed to a fluence² of 3×10^{14} $n_{\text{eq}}/\text{cm}^2$ per year at full luminosity. The irradiation dose will be a few times larger in the case of the LHC luminosity upgrade. The silicon sensors behavior will be determined by the radiation damage, which changes the electric field in the silicon bulk and introduces charge trapping. This will lead to a reduction of the collected charge [2]. The pixel detector will operate in a 4 T magnetic

field and charge carriers will be deflected by the Lorentz force, which enhances charge sharing between pixels and improves the spatial resolution. However, the bias voltage will be increased because of irradiation and the Lorentz deflection will be reduced [3]. The spatial resolution depends on the charge collection, track position, signal, noise and the Lorentz angle, and is degraded by irradiation. Here we present measurements of charge collection and Lorentz deflection as a function of depth in the silicon bulk for heavily irradiated pixel sensors. A new method for the extraction of the electric field in the silicon bulk is proposed and validated with a simple simulation.

*Corresponding author. Institut de Recherches Subatomiques, 23 rue du loess, BP28, F67037 Strasbourg. *E-mail address:* Andrei.Dorokhov@IReS.in2p3.fr

²All particle fluences are normalized to 1 MeV neutrons ($n_{\text{eq}}/\text{cm}^2$).

2. Sensors and the measurement technique

The sensors under study were designed for the CMS pixel detector and based on the “n-on-n” concept [4]. The bulk material is diffusively-oxygenated float zone (DOFZ) n-type silicon of (111) orientation and a resistivity 2-5 k Ω cm. The pixels are formed by p-spray isolated n⁺-implants, while the p-n junction is formed by a large p⁺-implant on the back side. The thickness of the sensor is 285 μ m and the pixel size is 125 \times 125 μ m². The sensors were irradiated at the CERN SPS with 24 GeV protons at room temperature without applying bias voltage and then stored at -20°C. The tests were carried out at the CERN H2 beam line with 150-225 GeV pions. The beam entered the pixel plane at a shallow angle $\alpha = 15^\circ$ and the 3 T magnetic field was parallel to the beam (see Fig. 1). The relationship between the z position of the created charge carriers and the corresponding arrival position at the pixel plane along the x axis is given by $z = x \tan \alpha$. Since the charge is always integrated in the pixel area, the smaller angle α is used the more precise location of charge carriers origin along the z axis is probed. The position of the beam exit point “O” was reconstructed in the pixel coordinates system using the beam telescope [5]. The beam telescope consisted of four modules, each containing two silicon strip sensors measuring the x and y coordinates. The strips had a pitch of 25 μ m, readout pitch of 50 μ m and the spatial resolution of each plane was about 1 μ m. The pixel sensors were bump-bonded to the PSI30/AC30 chip [6], which read out all signals from the 22 \times 32 pixel matrix. The pixel sensor was cooled by Peltier elements down to -10°C. Both pixel and beam telescope signals were digitized using VME-based ADC modules controlled by a DAQ software written in LabView and LabWindows/CVI (National Instruments). The trigger was provided by a PIN diode of size 3 \times 6 mm² placed between the beam telescope planes before the pixel detector.

The electrons and holes produced by particles crossing the pixel sensor drift toward the electrodes. In absence of magnetic field the electrons are collected along the segment \overline{OA} (see Fig. 1).

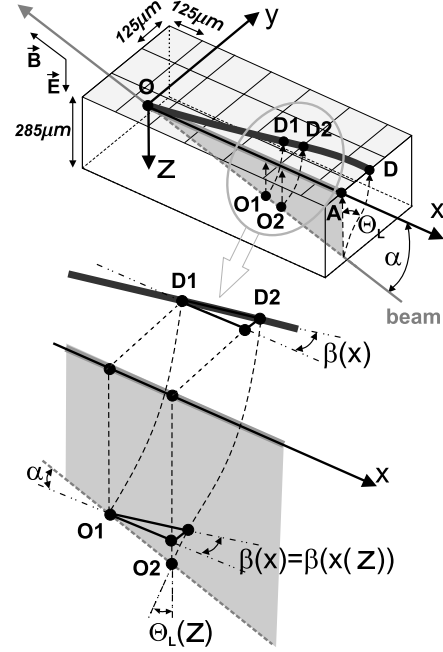


Figure 1. The deflection measurement technique.

The holes move to the opposite direction and, together with the electrons, induce the net current on the pixels situated along \overline{OA} . In presence of a magnetic field charge carriers are deflected by the Lorentz force and the resulting current is induced on the pixels along the segment \overline{OD} . This measurement technique was developed in [7] and used to measure the averaged Lorentz angle, Θ_L , by fitting the deflection \overline{OD} with a straight line. As we will see in section 3, the segment \overline{OD} is curved, because the Lorentz angle depends on the electric field, which changes over the depth. However, the experimental technique described in [7] can be applied for measuring the Lorentz angle as a function of depth in the sensor bulk. The bottom part of Fig. 1 shows the definition of $\beta(x)$ for an infinitely small section of the segment \overline{OD} . Knowing the beam incident angle $\alpha = 15^\circ$ and the deflection angle $\beta(x)$ the Lorentz angle at a certain depth $\Theta_L(z)$ is given by

$$\tan \Theta_L(z) = \frac{\tan \beta(x(z))}{\tan \alpha} = \tan \beta(x) / \tan \alpha. \quad (1)$$

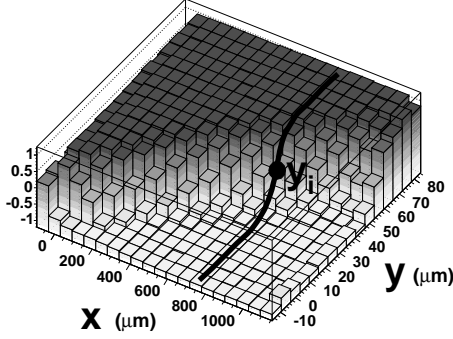


Figure 2. Asymmetry as a function of position in the xy plane for a non-irradiated sensor.

The angle α is known, therefore, the Lorentz angle is calculated in each point in depth with the tangent to the segment \overline{OD} , i.e. with the $\tan \beta(x)$. The geometrical position of the segment \overline{OD} in the xy coordinates plane can be determined from the signal asymmetry of two neighboring pixels. The asymmetry at the (x, y) position is defined as

$$A(x, y) = \frac{(Q_{x, y-p/2} - Q_{x, y+p/2})}{(Q_{x, y-p/2} + Q_{x, y+p/2})}, \quad (2)$$

where $Q_{x, y-p/2}$ and $Q_{x, y+p/2}$ is the charge collected in pixel, whose center is located at $(x, y - p/2)$ and $(x, y + p/2)$, respectively, and $p = 125 \mu\text{m}$ is the pixel size. The asymmetry averaged over all events in each (x, y) bin is shown in Fig. 2. The asymmetry plot was divided into slices along the x axis. The charge spread is approximated with the Gaussian function, therefore the asymmetry in the i -th slice located at x_i (e.g. represented by the solid line in Fig. 2) was fitted with the standard normal cumulative distribution function of y

$$A(x = x_i, y) = c \times \sqrt{\frac{2}{\pi}} \int_{-\infty}^{(y-y_i)/s} e^{-t^2/2} dt - c, \quad (3)$$

where the parameter y_i corresponds to the zero asymmetry position along the y coordinate for i -th slice (see Fig. 2), c and s are the constant and spread parameters of the fit. The set of points (y_i, x_i) determines the segment \overline{OD} . The $\tan \beta$ is determined from the derivative dy/dx . The slight

rotation (the line \overline{OA} can be rotated with respect to the pixel row) of the sensor in the xy plane was subtracted using the data without magnetic field. Each point x_i corresponds to a certain depth via the relation $z_i = x_i \tan \alpha$ and the deflection y_i can be expressed as a function of depth. The measured points were fitted with a 5-th order polynomial function (see Fig. 4).

3. Charge collection and the Lorentz deflection

Measurements without magnetic field were performed to determine the signal distribution along the segment \overline{OA} see Fig. 1. Assuming the averaged energy loss along the particle track to be uniform, the average signal in a pixel along \overline{OA} is proportional to the charge collection efficiency originating at a certain depth in the silicon bulk. The average charge collected by a single pixel as a function of the pixel position along \overline{OA} is shown in Fig. 3 for a sensor irradiated at $6.7 \times 10^{14} \text{ n}_{\text{eq}}/\text{cm}^2$. One can see, that even at low bias voltage (100-200V) some charge is collected from the p^+ side and the charge has a minimum in the middle of the sensor thickness. Most of the charge, however, comes from the region close to the pixel implant. This behavior can be explained

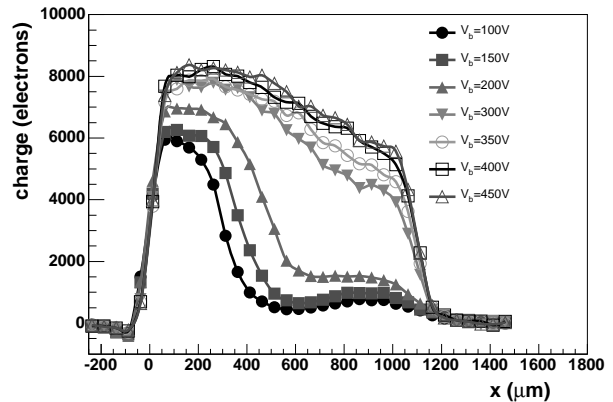


Figure 3. Average collected charge as a function of the distance to the exit point for a sensor irradiated at $6.7 \times 10^{14} \text{ n}_{\text{eq}}/\text{cm}^2$ for different bias voltages.

by a non-linear electric field and by trapping of charge carriers. If the sensor is operated in a magnetic field, the charge carriers are deflected by the Lorentz angle Θ_L . The signal is induced on the pixels along the segment \overline{OD} (see Fig. 1). Since the electric field in irradiated sensor is not linear, the segment between the points “O” and “D” is curved, and in each point its tangent determines the deflection angle β . The deflection of collected charge along the y axis as a function of the depth in the silicon bulk is shown in Fig.4 for different fluences and bias voltages. It must be noticed,

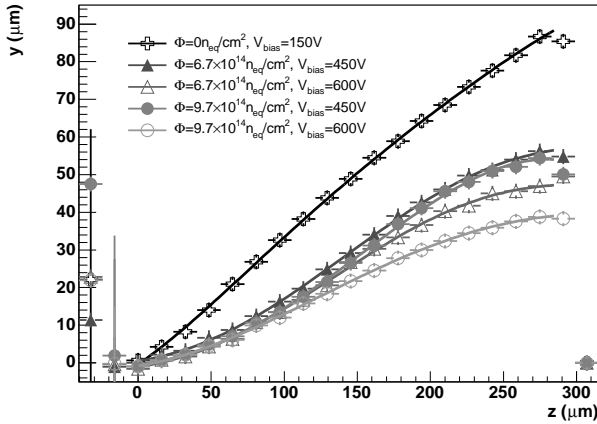


Figure 4. Lorentz deflection of the charge in a 3 T magnetic field as a function of the depth.

that at the edges of the silicon bulk ($z < 17\mu\text{m}$ or $z > 268\mu\text{m}$) the measured deflection has high systematic uncertainties (not shown in Fig. 4) due to the geometrical distortions of the electric field lines and incorrect reconstruction of the deflection curve \overline{OD} . The errors due to the particles multiple scattering were eliminated by selecting only straight tracks reconstructed by the beam telescope.

4. Electric field measurements

4.1. Electric field strength across the silicon bulk

In case of small Lorentz angles the low magnetic field approximation can be used to describe the charge carriers motion in crossed electric and magnetic fields. This approximation physically

corresponds to the situation where charge carriers travel only for a small arc of the circular orbit before scattering moves them from this orbit into another. The general expression of the current density in presence of crossed electric and magnetic fields can be found in [8]. The Lorentz angle can be obtained from the direction of the current density as

$$\tan \Theta_L = r_h \mu B, \quad (4)$$

where r_h is the Hall factor, B is the magnetic field and μ is the drift mobility. The charge carriers mobility is determined by the lattice and impurity scattering. At the temperatures around 300 K and for the impurity concentration up to 10^{18} cm^{-3} the major contribution to the mobility is from lattice scattering. For the impurity concentration up to 10^{15} cm^{-3} the impurity scattering contribution to the total mobility is below one percent and the Hall factor changes less than one percent in the range of impurity concentration from 10^{13} cm^{-3} to 10^{15} cm^{-3} [9]. Assuming that the irradiation induced defects act as impurity atoms, the influence of irradiation on the mobility and Hall factor can be neglected for all irradiated sensors used for the tests. Therefore the measured Lorentz angle can be used to calculate the mobility using the Eq. 4. Most of the signal is due to the electrons contribution due to their shorter collection time and due to specific shape of the effective potential which is confirmed by the simulation (see Fig. 7 and Fig. 8). Moreover, despite the fact that holes are also deflected during their drift, they will arrive to the backside which has the same effective potential used to calculate the induced current on pixels using the Ramo-Shockley theorem [10]. Therefore the signal induced by holes will be on the line \overline{OA} even in presence of magnetic field and will not disturb the measured line \overline{OD} which is only due to the collected electrons. Using the measured $\Theta_L(z)$ ($\tan \Theta_L$ is a derivative of the deflection shown in Fig. 4) and using Eq. 4, the electron mobility as a function of the depth is given by

$$\mu_e(z) = \frac{\tan \Theta_L(z)}{r_h B_x}, \quad (5)$$

where $r_h = 1.15$ is the Hall factor for the electrons and $B_x = (3 \cos(15^\circ))$ T is the projection of the magnetic field along the x axis. The measured

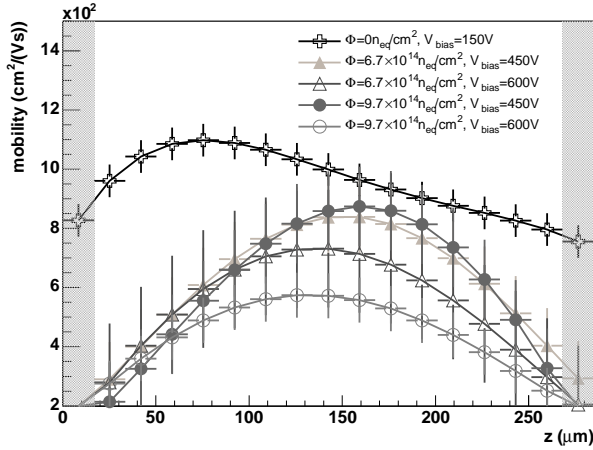


Figure 5. Measured electrons mobility as a function of depth for different fluences and bias voltages. The shaded regions correspond to the depth values where the mobility has large systematic uncertainties.

electron mobility as a function of the sensor depth is shown in Fig.5 for different fluences and bias voltages.

Using empirical parameterization of the field dependence of the electron mobility [11] and [12], one can derive the electric field as a function of the depth

$$E(z) = E_{ce} \left[\left(\frac{\mu_{0e}}{\mu_e(z)} \right)^{\gamma_e} - 1 \right]^{1/\gamma_e}, \quad (6)$$

where μ_e is the measured electron mobility and μ_{0e} (low electric field electron mobility), E_{ce} and γ_e are known empirical parameters from [11] and [12]. The parametrized mobility agrees within 5% with the measured mobilities [12]. The relative error of the electric field r_E calculated using Eq. 6 is related to relative error of the mobility r_μ as

$$r_E = r_\mu \frac{1}{1 - \left(\frac{\mu}{\mu_0} \right)^\gamma}. \quad (7)$$

For the expected mobility range the error of the electric field extraction method is between 5 and

15%. Fig. 6 shows the electric field obtained neglecting the electric field lines distortion close to the pixel implants. The measurement is restricted to the depth range $17 \mu\text{m} < z < 268 \mu\text{m}$ for the reasons explained in section 3. The errors shown in Fig. 6 are attributed to statistical fluctuation of the collected charge and do not include the error of the electric field extraction method, which is below 15%. For the non-irradiated sensor the

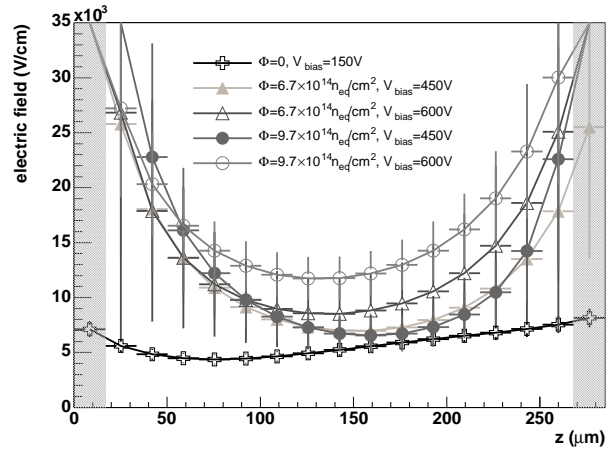


Figure 6. Extracted electric field as a function of depth for the non-irradiated and irradiated silicon sensors at different bias voltages. The shaded regions correspond to the depth values where the electric field has large systematic uncertainties.

electric field is close to the classical linear field of an abrupt p-n junction. For the heavily irradiated sensors the electric field has a double peak with a distinct minimum close to the middle of the bulk. The origin of the double-peak electric field is qualitatively described in [13]. A two-trap model producing a doubly-peaked electric field was implemented in a detailed detector simulation and the simulated charge collection was found to be in good agreement with the measurements [14,15]. By integrating the electric field over the depth one can determine the potential drop across the silicon bulk. The potential drop agrees with the applied bias voltage within 15% for all sensors.

4.2. Cross-check of the measured electric field

In order to check the measured electric field a simulation of the signal induced in the pixels was performed. The particle crosses the silicon sensor with an angle $\alpha = 15^\circ$ (see Fig.1) and the energy loss is assumed to be uniformly distributed. Neither energy loss fluctuation nor charge diffusion was taken into account. In this simulation the electric field lines are assumed to be perpendicular to the silicon sensor planes and the electric field value as function of the depth was taken from the measurement shown in Fig. 6. The time dependent induced current is calculated using the Shockley-Ramo theorem [10]

$$i(t) = Q_h(t)\vec{G}[z(t)] \cdot \vec{v}_h[z(t)] + Q_e(t)\vec{G}[z(t)] \cdot \vec{v}_e[z(t)], \quad (8)$$

where Q_h and Q_e are the holes and electrons charge values deposited by the particle energy loss, respectively, \vec{G} is the weighting field, \vec{v}_h and \vec{v}_e the holes and electrons drift velocities, respectively.

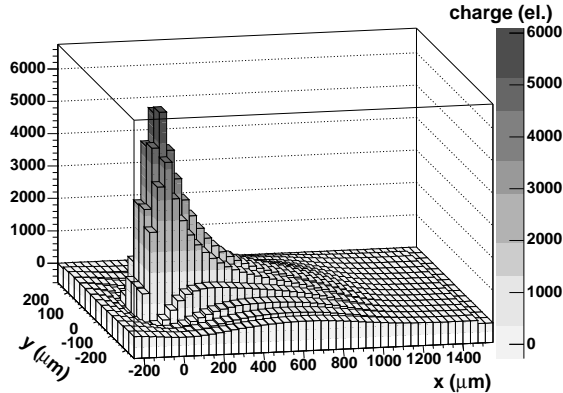


Figure 7. Simulated signal induced by holes.

The drift velocity is calculated using the measured electric field and the electrons and holes are trapped during the drifting time according to the exponential law

$$Q_h(t) = Q_{0h}e^{-t/\tau_h}, \quad Q_e(t) = Q_{0e}e^{-t/\tau_e}, \quad (9)$$

where the fluence dependent trapping probabilities τ_h^{-1} and τ_e^{-1} are calculated assuming a lin-

ear dependence on irradiation fluence. The proportionality coefficients are $4.2 \times 10^{-16} \text{ cm}^2/\text{ns}$ for electrons and $6.1 \times 10^{-16} \text{ cm}^2/\text{ns}$ for holes respectively [16]. For the non-irradiated sensors the trapping probability is set to zero, as the collection time is in the order of few nanoseconds. The induced signal was calculated separately for

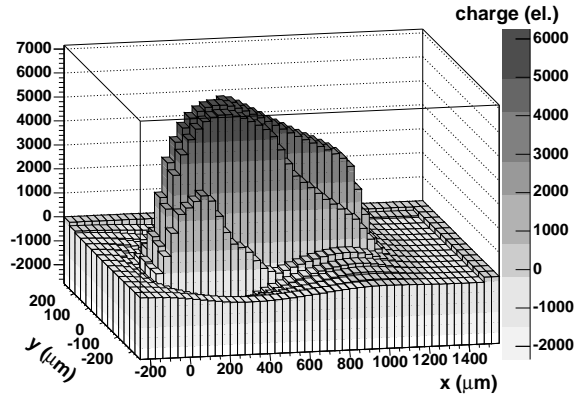


Figure 8. Simulated signal induced by electrons.

holes (see Fig. 7) and electrons (see Fig. 8) taking into account the Lorentz force. The total induced signal is shown in Fig. 9. The contribution from holes is significant only at the region close to the pixel implant while the total induced current is dominated by electrons. Figure 10 shows

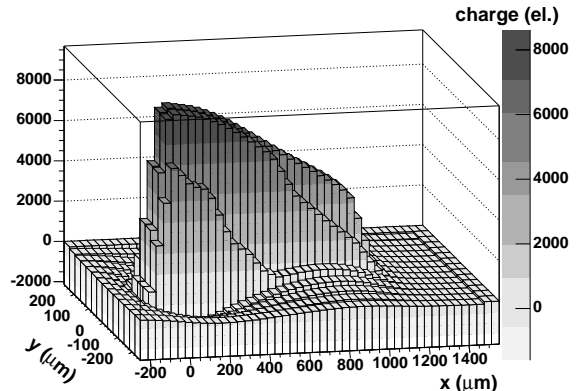


Figure 9. Simulated total induced signal along the particle track projection with a magnetic field of $(3 \cos(15^\circ)) \text{ T}$.

the measured and simulated deflection as function of depth. The charge deflection predicted by the simulation reproduces the measurements well. The simulation was performed also with-

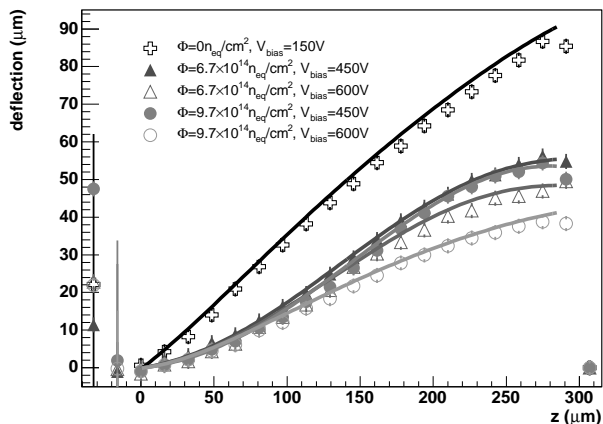


Figure 10. Measured (markers) and simulated (solid lines) deflection as a function of depth for different fluences and bias voltages.

out magnetic field to compare the charge collection efficiency with the measurement. The simulation reproduces the measured values very well (see Fig. 11). The small discrepancies are due to charge diffusion, energy deposit fluctuation, electric field distortion between the implants which were not implemented in the simulation.

5. Summary

A new method to extract the electric field in irradiated silicon pixel sensors is proposed and validated with a simulation. The method is based on a precise measurement of the Lorentz deflection as a function of depth in the silicon sensor bulk. The extracted electric field is used in a sensor simulation which reproduces very well both the charge collection and the Lorentz deflection. The method uses the electric field dependency on the mobility. Therefore, the precision of the method is limited by the precision of this dependence. However the empirical dependence agrees with the measurements very well [12] and the error on the electric field is estimated to be less

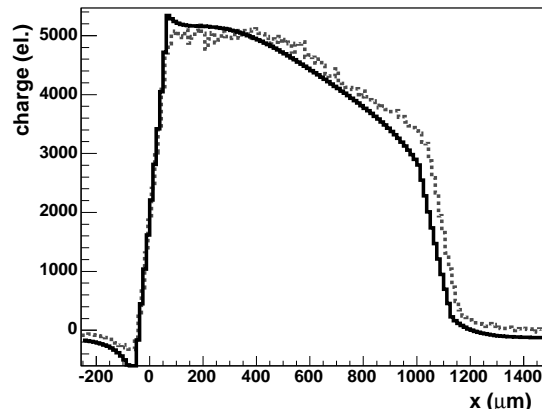


Figure 11. Charge collected along the particle track for a sensor irradiated at $6.7 \times 10^{14} \text{ n}_{\text{eq}}/\text{cm}^2$. The solid line is the simulated charge, dashed line is the measured one.

than 15%.

The Lorentz angle is used for mobility calculation and the error of the Lorentz angle measurements is dominated by the statistical fluctuations of the collected charge. The influence of the irradiation on the mobility and the Hall factor can be neglected for fluences up to $10^{15} \text{ n}_{\text{eq}}/\text{cm}^2$ because of the lattice scattering dominates over the scattering on the irradiation induced defects.

Acknowledgments

We gratefully acknowledge Silvan Streuli from ETH Zurich and Fredy Glaus from PSI for their immense effort on the bump bonding of the pixel sensors. We would like to thank Maurice Glaser and Michael Moll from CERN for carrying out the irradiation, Kurt Bösiger from the Zürich workshop for the mechanical construction, György Bencze and Pascal Petiot from CERN for the H2 beam line support and finally the whole CERN-SPS team.

REFERENCES

1. CMS Collaboration, CMS TDR 5, CERN-LHCC-1998-06, 1998.
2. T. Rohe *et al.*, 5th Int. Conf. on Rad. Effects on Sem. Mater. Det. and Devices, Oct. 10-

- 13, 2004, Florence, Italy, submitted to Nucl. Instr. and Meth. in Phys. Research A, e-print arXiv:physics/0411214.
3. A. Dorokhov *et al.*, Nucl. Instr. and Meth. in Phys. Research A **530** Issues 1-2, (2004) 71-76.
 4. T. Rohe *et al.*, IEEE-NSS, October 19-25, 2003, Portland, Oregon, USA, IEEE-TNS 51-3 (2004).
 5. C. Amsler *et al.*, Nucl. Instr. and Meth. in Phys. Research A **480** (2002) 501.
 6. D. Meer, Bau und Messen eines Multi-chip Pixelmodules
als Prototyp für den CMS Tracker, Diploma Thesis,
ETH Zürich, March 2000.
 7. B. Henrich, R. Kaufmann, Nucl. Instr. and Meth. in Phys. Research A **477** (2002) 304.
 8. R. H. Bube, Electronic Properties of Crystalline Solids, An introduction to fundamentals, Academic Press, INC, 1974.
 9. P. Norton, T. Braggins and H. Levinstein, Phys. Rev., vol. B8, no. 12, (1973) 5632.
 10. W. Shockley, J. Appl. Phys. 9, (1938) 635
S. Ramo, Proc. IRE 27, (1939) 584.
 11. N. D. Arora, J. R. Hauser, D. J. Roulston
IEEE Trans. Electron Devices, ED-29, 292, 1982.
 12. D. M. Caughey and R. F. Thomas, Proc. IEEE, vol. 55 (Dec. 1967) 2192.
 13. V. Eremin, E. Verbitskaya, Z. Li, Nucl. Instr. and Meth. in Phys. Research A **476** (2002) 556.
 14. M. Swartz, Nucl. Instr. and Meth. in Phys. Research A **511** Issues 1-2, (2003) 88-91.
 15. V. Chiochia *et al.*, IEEE Nuclear Science Symposium, October 18-21, Rome, Italy, Submitted to IEEE-TNS, e-print arXiv:physics/0411143.
 16. G. Kramberger, V. Cindro, I. Mandic, M. Mikuz and M. Zavrtanik, Nucl. Instr. and Meth. in Phys. Research A **476** Issue 3, (2002) 645-651.